

Quaternion higher-order singular value decomposition and its applications in color image processing

Jifei Miao and Kit Ian Kou

Abstract—Higher-order singular value decomposition (HOSVD) is one of the most efficient tensor decomposition techniques. It has the salient ability to represent high-dimensional data and extract features. In more recent years, the quaternion has proven to be a very suitable tool for color pixel representation as it can well preserve cross-channel correlation of color channels. Motivated by the advantages of the HOSVD and the quaternion tool, in this paper, we generalize the HOSVD to the quaternion domain and define quaternion-based HOSVD (QHOSVD). Due to the non-commutability of quaternion multiplication, QHOSVD is not a trivial extension of the HOSVD. They have similar but different calculation procedures. The defined QHOSVD can be widely used in various visual data processing with color pixels. In this paper, we present two applications of the defined QHOSVD in color image processing—multi-focus color image fusion and color image denoising. The experimental results on the two applications respectively demonstrate the competitive performance of the proposed methods over some existing ones.

Index Terms—Quaternion higher-order singular value decomposition (QHOSVD), quaternion tensor, multi-focus color image fusion, color image denoising.

I. INTRODUCTION

Higher-order singular value decomposition (HOSVD) is a natural extension of the singular value decomposition (SVD) in higher dimensional space [1]. Benefiting from the outstanding ability of high-dimensional data representing and feature extracting, the HOSVD has been widely applied in many areas such as image fusion [2], face recognition [3], texture synthesis [4], image denoising [5], *etc.* On the other hand, quaternion, as an elegant color image representation tool, has attracted much attention in the field of color image processing, recently. For instance, it has achieved excellent results in color image filtering [6], color image edge detection [7], color image denoising [8], [9], color face recognition

[10], [11], color image inpainting [12], [13] and so on. However, most of the existing quaternion-based methods are limited to one-dimensional quaternion vector or two-dimensional quaternion matrix. Although they can perfectly preserve the connection between color channels, they cannot make good use of the spatial structure of higher dimensional data. Thus, in this paper, combining the advantages of HOSVD and quaternion, we aim to define quaternion-based HOSVD (QHOSVD) and use it for color image processing.

HOSVD was first defined by De Lathauwer et al. in [1], which is a proper generalization of the SVD. The HOSVD of a tensor $\mathcal{T} \in \mathbb{R}^{N_1 \times N_2 \times \dots \times N_L}$ is given by

$$\mathcal{T} = \mathcal{S} \times_1 \mathbf{U}_1 \times_2 \mathbf{U}_2 \dots \times_L \mathbf{U}_L,$$

where $\mathbf{U}_l \in \mathbb{R}^{N_l \times N_l}$ ($l = 1, \dots, L$) are orthogonal matrices, $\mathcal{S} \in \mathbb{R}^{N_1 \times N_2 \times \dots \times N_L}$ is called the core tensor. Following the calculation procedure in [1], the core tensor \mathcal{S} satisfies the all-orthogonality conditions¹. The concept of QHOSVD, in this paper, is an extension of the HOSVD on quaternions, but the limitation of non-commutativity of quaternion multiplication results in the definition and calculation procedure of QHOSVD cannot be the same as that of HOSVD. It should be noted that the definition of QHOSVD is application-oriented. The defined QHOSVD can be widely used in various visual data processing with color pixels. As examples, in this paper, we tend to use it to solve two common color image processing problems: multi-focus color image fusion and color image denoising.

Multi-focus image fusion is an effective technique to extend the depth-of-field of optical lenses by creating an all-in-focus image from a set of partially focused images of the same scene [14]. The existing multi-focus image fusion methods can be roughly classified into three categories: Transform domain methods, *e.g.*, [2], [15]–[18], spatial domain methods, *e.g.*, [19]–[21],

The authors are with the Department of Mathematics, Faculty of Science and Technology, University of Macau, Macau 999078, China (e-mail: jifmiao@163.com; kikou@umac.mo)

¹We will introduce the concept of all-orthogonality hereinafter. For more information about HOSVD, readers can refer to [1].

and deep learning methods, *e.g.*, [22], [23]. Most of the existing traditional methods are inherently designed for multi-focus grayscale image fusion. For color multi-focus images, they generally fuse three color channels independently. Quaternions have also been widely used in this field in the past few years. For example those in [24]–[26], which mainly focus on grayscale images. In [27] and [28], the authors respectively using quaternion wavelet transform (QWT) and quaternion curvelet transform (QCT) to fuse multi-focus color images. However, the fixed base of QWT and QCT usually cannot obtain accurate features of color images. Motivated by the fact that HOSVD, an efficient data-driven decomposition technique, can obtain a dynamic adaptive base [5], and it has the salient ability for feature extraction [29], we design a novel multi-focus color image fusion method based on the defined QHOSVD procedure. In consideration of the fact that image fusion mainly depends on local information of source images [29], the source images are firstly divided into image patches using the sliding window technique. Then, since these partially focused color images refer to the same scene and are highly similar, we construct them (represented as quaternion matrices) into a third-order quaternion tensor [30] and adopt the proposed QHOSVD procedure to extract their features simultaneously. Then, The L_1 -norm of the coefficient quaternion sub-tensor is employed as the activity measure and the maximum selection fusion rule is adopted to obtain the fused coefficient quaternion sub-tensor. To construct the entire fused image, all the fused patches are pasted in their corresponding positions and the intensity value of an overlapped pixel is averaged by its accumulative times.

Recently, quaternion has also been applied to color image denoising, and achieved promising results. For example, the authors in [9] and [8] extended the traditional low-rank matrix approximation methods to the quaternion domain and respectively proposed low-rank quaternion approximation (LRQA) (including nuclear norm, Laplace function, Geman function, and weighted Schatten norm) and quaternion weighted nuclear norm minimization (QWNNM) algorithms. The nonlocal self-similarity (NSS) of the color image is exploited in these methods to promote the denoising performance. However, these methods will destroy the two-dimensional spatial structure of color image patches when they are expanded into one-dimensional column quaternion vectors. Aiming at this drawback of the existing quaternion matrix-based methods, we propose a novel color image denoising method based on the defined QHOSVD. Selected similar color image patches (represented as quaternion matrices) are stacked into a third-order quaternion

tensor, and then the proposed QHOSVD procedure is performed on it to obtain the singular value coefficients. Finally, manipulate these coefficients by noise level related hard thresholding, and invert the QHOSVD procedure to produce the denoised color image patches used to construct the final full denoised color image.

The main contributions of this paper can be summarized as follows.

- We generalize the concept of the HOSVD to the quaternion domain and define QHOSVD. We also give the calculation procedure of the QHOSVD, which is different from that of HOSVD in [1].
- Based on the defined QHOSVD, we propose a novel multi-focus color image fusion method and a novel color image denoising method.
- Both methods are used to deal with the corresponding color image processing tasks. The experimental results on both problems demonstrate their competitive performance.

The remainder of this paper is organized as follows. Section II introduces some notations and preliminaries for quaternion algebra. Section III introduces the quaternion tensors and the related definitions, operations, and properties. Section IV gives the definition of QHOSVD and the detailed calculation procedure. Section V presents two applications of the defined QHOSVD in color image processing, including multi-focus color image fusion and color image denoising. Section VI provides some experiments to illustrate the performance of the proposed corresponding color image processing methods. Finally, some conclusions are drawn in Section VII.

II. NOTATIONS AND PRELIMINARIES

In this section, we first summarize some main notations and then introduce some basic knowledge of quaternion algebra.

A. Notations

In this paper, \mathbb{R} , \mathbb{C} , and \mathbb{H} respectively denote the real space, complex space, and quaternion space. A scalar, a vector, a matrix, and a tensor are written as a , \mathbf{a} , \mathbf{A} , and \mathcal{A} respectively. \hat{a} , $\hat{\mathbf{a}}$, $\hat{\mathbf{A}}$, and $\hat{\mathcal{A}}$ respectively represent a quaternion scalar, a quaternion vector, a quaternion matrix, and a quaternion tensor. The (n_1, n_2) th and the (n_1, n_2, \dots, n_L) th entries in $\hat{\mathbf{A}} \in \mathbb{H}^{N_1 \times N_2}$ and $\hat{\mathcal{A}} \in \mathbb{H}^{N_1 \times N_2 \times \dots \times N_L}$ are respectively denoted as $\hat{a}_{n_1 n_2}$ and $\hat{a}_{n_1 n_2 \dots n_L}$. The mode- k unfolding of a quaternion tensor \mathcal{A} is denoted by $\text{Unfold}_k(\mathcal{A}) := \hat{\mathbf{A}}_{[k]} \times_k \otimes$, and $\langle \cdot, \cdot \rangle$ respectively denote the k -mode product, Kronecker product, and inner product. $(\cdot)^*$, $(\cdot)^T$, and

$(\cdot)^H$ denote the conjugation, transpose, and conjugate transpose, respectively. $|\cdot|$, $\|\cdot\|_F$ and $\|\cdot\|_{L_1}$ are respectively the modulus, Frobenius norm, and L_1 norm.

B. Basic knowledge of quaternion algebras

Quaternion space \mathbb{H} was first introduced by W. Hamilton [31] in 1843, which is an extension of the complex space \mathbb{C} . Some basic knowledge of quaternion algebras can be found in Appendix A. In the following, we give some properties used in this paper about quaternion matrices.

Theorem 1. *Given two quaternion matrices $\dot{\mathbf{A}} \in \mathbb{H}^{M \times N}$ and $\dot{\mathbf{B}} \in \mathbb{H}^{N \times M}$. Then*

- (a) $(\dot{\mathbf{A}}\dot{\mathbf{B}})^H = \dot{\mathbf{B}}^H\dot{\mathbf{A}}^H$ [32];
- (b) $(\dot{\mathbf{A}}\dot{\mathbf{B}})^* \neq \dot{\mathbf{A}}^*\dot{\mathbf{B}}^*$ in general [32];
- (c) $(\dot{\mathbf{A}}\dot{\mathbf{B}})^T \neq \dot{\mathbf{B}}^T\dot{\mathbf{A}}^T$ in general [32];
- (d) If $\dot{\mathbf{A}}$ is unitary (i.e., $\dot{\mathbf{A}}^H\dot{\mathbf{A}} = \mathbf{I}$), $\dot{\mathbf{A}}^*$ and $\dot{\mathbf{A}}^T$ are generally no longer unitary.

One can directly verify (d) based on (a) and (c).

III. QUATERNION TENSORS

Quaternion tensors are generalizations of quaternion vectors (that have one index) and quaternion matrices (that have two indices) to an arbitrary number of indices. The notation about quaternion tensors used here is very similar to that of the real-valued case in [33].

Definition 1. *(Quaternion tensor [30]) A multidimensional array or an L th-order tensor is called a quaternion tensor if its entries are quaternion numbers, i.e.,*

$$\begin{aligned} \dot{\mathcal{T}} &= (\dot{t}_{n_1 n_2 \dots n_L}) \in \mathbb{H}^{N_1 \times N_2 \times \dots \times N_L} \\ &= \mathcal{T}_0 + \mathcal{T}_1 i + \mathcal{T}_2 j + \mathcal{T}_3 k, \end{aligned} \quad (1)$$

where $\mathcal{T}_p \in \mathbb{R}^{N_1 \times N_2 \times \dots \times N_L}$ ($p = 0, 1, 2, 3$), $\dot{\mathcal{T}}$ is named a pure quaternion tensor when \mathcal{T}_0 is a zero tensor.

Definition 2. *(Mode- k unfolding [30]) For an L th-order quaternion tensor $\dot{\mathcal{T}} \in \mathbb{H}^{N_1 \times N_2 \times \dots \times N_L}$, its mode- k unfolding is denoted by $\dot{\mathbf{T}}_{[k]}$ and arranges the mode- k fibers to be the columns of the quaternion matrix, i.e.,*

$$\text{Unfold}_k(\dot{\mathcal{T}}) = \dot{\mathbf{T}}_{[k]} \in \mathbb{H}^{N_k \times N_1 \dots N_{k-1} N_{k+1} \dots N_L}$$

with entries

$$\dot{\mathbf{T}}_{[k]}(n_k, n_1 \dots n_{k-1} n_{k+1} \dots n_L) = \dot{t}_{n_1 n_2 \dots n_L},$$

where $\dot{t}_{n_1 n_2 \dots n_L}$ is the (n_1, n_2, \dots, n_L) th entry of $\dot{\mathcal{T}}$.

Definition 3. *(The k -mode product) The k -mode product of a quaternion tensor $\dot{\mathcal{T}} \in \mathbb{H}^{N_1 \times N_2 \times \dots \times N_L}$ with a*

matrix $\dot{\mathbf{U}} \in \mathbb{H}^{M \times N_k}$ is denoted by² $\dot{\mathcal{Y}} = \dot{\mathcal{T}} \times_k \dot{\mathbf{U}} \in \mathbb{H}^{N_1 \times \dots \times N_{k-1} \times M \times N_{k+1} \times \dots \times N_L}$ with entries

$$\dot{y}_{n_1 \dots n_{k-1} m n_{k+1} \dots n_L} = \sum_{n_k=1}^{N_k} \dot{u}_{m n_k} \dot{t}_{n_1 n_2 \dots n_L}. \quad (2)$$

From **Definition 3**, we can find the following facts:

- ❶ The k -mode product can also be expressed in terms of unfolded quaternion tensors:

$$\dot{\mathcal{Y}} = \dot{\mathcal{T}} \times_k \dot{\mathbf{U}} \iff \dot{\mathbf{Y}}_{[k]} = \dot{\mathbf{U}} \dot{\mathbf{T}}_{[k]}.$$

- ❷ If the modes are the same, then

$$\dot{\mathcal{T}} \times_k \dot{\mathbf{U}}_1 \times_k \dot{\mathbf{U}}_2 = \dot{\mathcal{T}} \times_k (\dot{\mathbf{U}}_2 \dot{\mathbf{U}}_1).$$

- ❸ For distinct modes in a series of multiplications, the sequence of the multiplication is vitally important, i.e., if $k_1 \neq k_2$, generally

$$\dot{\mathcal{T}} \times_{k_1} \dot{\mathbf{U}}_1 \times_{k_2} \dot{\mathbf{U}}_2 \neq \dot{\mathcal{T}} \times_{k_2} \dot{\mathbf{U}}_2 \times_{k_1} \dot{\mathbf{U}}_1.$$

- ❹ If $\dot{\mathcal{Y}} = \dot{\mathcal{T}} \times_1 \dot{\mathbf{U}}_1 \times_2 \dot{\mathbf{U}}_2 \dots \times_L \dot{\mathbf{U}}_L$, then

$$\dot{\mathbf{Y}}_{[L]} = \dot{\mathbf{U}}_L \left((\dot{\mathbf{U}}_{L-1} \otimes \dots \otimes \dot{\mathbf{U}}_1) \dot{\mathbf{T}}_{[L]}^T \right)^T$$

but for $k \neq L$, generally

$$\begin{aligned} \dot{\mathbf{Y}}_{[k]} &\neq \dot{\mathbf{U}}_k \left((\dot{\mathbf{U}}_L \otimes \dots \otimes \dot{\mathbf{U}}_{k+1} \otimes \dot{\mathbf{U}}_{k-1} \right. \\ &\quad \left. \otimes \dots \otimes \dot{\mathbf{U}}_1) \dot{\mathbf{T}}_{[k]}^T \right)^T. \end{aligned}$$

Facts ❶ and ❷ are the same as their real-valued counterparts [33]. However, due to the non-commutativity of quaternion multiplication, and the property of quaternion matrix (see **Theorem 1** (c)), facts ❸ and ❹ are completely different from their real-valued counterparts.

IV. QUATERNION HIGHER ORDER SINGULAR VALUE DECOMPOSITION

The HOSVD is one of the most efficient tensor decomposition techniques [1]. Motivated by the outstanding ability of the HOSVD to represent high-dimensional data and extract features, in this section, we try to generalize the HOSVD to the quaternion domain and define QHOSVD.

Theorem 2. *Every quaternion tensor $\dot{\mathcal{T}} \in \mathbb{H}^{N_1 \times N_2 \times \dots \times N_L}$ can be written as the form*

$$\dot{\mathcal{T}} = \dot{\mathcal{S}} \times_1 \dot{\mathbf{U}}_1 \times_2 \dot{\mathbf{U}}_2 \dots \times_L \dot{\mathbf{U}}_L, \quad (3)$$

where $\dot{\mathbf{U}}_l \in \mathbb{H}^{N_l \times N_l}$ ($l = 1, \dots, L$) are unitary quaternion matrices, $\dot{\mathcal{S}} \in \mathbb{H}^{N_1 \times N_2 \times \dots \times N_L}$ is a quaternion

²It should be noted that different from the definition of the real-valued case in [33], the sequence of $\dot{u}_{m n_k}$ and $\dot{t}_{n_1 n_2 \dots n_L}$ in (2) is not commutative, which is determined by the non-commutativity of quaternion multiplication.

tensor with the same size as $\dot{\mathcal{T}}$. The quaternion sub-tensors $\dot{\mathcal{S}}_{n_l=\alpha}$ obtained by fixing the l th index of $\dot{\mathcal{S}}$ to α have the property that

$$\|\dot{\mathcal{S}}_{n_l=1}\|_F \geq \|\dot{\mathcal{S}}_{n_l=2}\|_F \geq \dots \geq \|\dot{\mathcal{S}}_{n_l=N_l}\|_F \geq 0. \quad (4)$$

proof. From fact **4**, equation (3) can be expressed in a quaternion matrix format as

$$\dot{\mathbf{T}}_{[L]} = \dot{\mathbf{U}}_L \left((\dot{\mathbf{U}}_{L-1} \otimes \dots \otimes \dot{\mathbf{U}}_1) \dot{\mathbf{S}}_{[L]}^T \right)^T. \quad (5)$$

Now consider the particular case where $\dot{\mathbf{U}}_L$ is obtained from the QSVD of $\dot{\mathbf{T}}_{[L]}$ as

$$\dot{\mathbf{T}}_{[L]} = \dot{\mathbf{U}}_L \boldsymbol{\Sigma}_L \dot{\mathbf{V}}_L^H. \quad (6)$$

Equation (3) can then be expressed in a quaternion matrix format as

$$\text{Unfold}_{L-1}(\dot{\mathcal{T}} \times_L \dot{\mathbf{U}}_L^H) = \dot{\mathbf{U}}_{L-1} \left((\dot{\mathbf{U}}_{L-2} \otimes \dots \otimes \dot{\mathbf{U}}_1) \dot{\mathbf{S}}_{[L-1]}^T \right)^T. \quad (7)$$

Then, the particular case where $\dot{\mathbf{U}}_{L-1}$ is obtained from the QSVD of $\text{Unfold}_{L-1}(\dot{\mathcal{T}} \times_L \dot{\mathbf{U}}_L^H)$ as

$$\text{Unfold}_{L-1}(\dot{\mathcal{T}} \times_L \dot{\mathbf{U}}_L^H) = \dot{\mathbf{U}}_{L-1} \boldsymbol{\Sigma}_{L-1} \dot{\mathbf{V}}_{L-1}^H. \quad (8)$$

Continue the above procedure in sequence, and equation (3) finally can be expressed in a quaternion matrix format as

$$\text{Unfold}_1(\dot{\mathcal{T}} \times_L \dot{\mathbf{U}}_L^H \times_{L-1} \dot{\mathbf{U}}_{L-1}^H \dots \times_2 \dot{\mathbf{U}}_2^H) = \dot{\mathbf{U}}_1 \dot{\mathbf{S}}_{[1]}. \quad (9)$$

The particular case where $\dot{\mathbf{U}}_1$ is obtained from the QSVD of $\text{Unfold}_1(\dot{\mathcal{T}} \times_L \dot{\mathbf{U}}_L^H \times_{L-1} \dot{\mathbf{U}}_{L-1}^H \dots \times_2 \dot{\mathbf{U}}_2^H)$ as

$$\text{Unfold}_1(\dot{\mathcal{T}} \times_L \dot{\mathbf{U}}_L^H \times_{L-1} \dot{\mathbf{U}}_{L-1}^H \dots \times_2 \dot{\mathbf{U}}_2^H) = \dot{\mathbf{U}}_1 \boldsymbol{\Sigma}_1 \dot{\mathbf{V}}_1^H. \quad (10)$$

Afterwards, the quaternion tensor $\dot{\mathcal{S}}$ can be obtained by

$$\dot{\mathcal{S}} = \dot{\mathcal{T}} \times_L \dot{\mathbf{U}}_L^H \times_{L-1} \dot{\mathbf{U}}_{L-1}^H \dots \times_1 \dot{\mathbf{U}}_1^H. \quad (11)$$

Then, taking $\dot{\mathcal{S}}_{n_L}$ as an example, we show the property (4). Comparing (5) and (6), we can find that

$$\dot{\mathbf{S}}_{[L]} = \boldsymbol{\Sigma}_L \left(\dot{\mathbf{V}}_L^T (\dot{\mathbf{U}}_{L-1} \otimes \dots \otimes \dot{\mathbf{U}}_1) \right)^*, \quad (12)$$

in which $\boldsymbol{\Sigma}_L = \text{diag}(\sigma_L^{(1)}, \sigma_L^{(2)}, \dots, \sigma_L^{(N_L)})$, where

$$\sigma_L^{(1)} \geq \sigma_L^{(2)} \geq \dots \geq \sigma_L^{(N_L)} \geq 0. \quad (13)$$

We call r_L the highest index for which $\sigma_L^{r_L} > 0$, which combining (13) means³

$$\|\dot{\mathcal{S}}_{n_L=1}\|_F \geq \|\dot{\mathcal{S}}_{n_L=2}\|_F \geq \dots \geq \|\dot{\mathcal{S}}_{n_L=r_L}\|_F, \quad (14)$$

³Note that $\dot{\mathbf{V}}_L$ and $(\dot{\mathbf{U}}_{L-1} \otimes \dots \otimes \dot{\mathbf{U}}_1)$ are unitary, thus the Frobenius norm of each row vector of $(\dot{\mathbf{V}}_L^T (\dot{\mathbf{U}}_{L-1} \otimes \dots \otimes \dot{\mathbf{U}}_1))^*$ is 1.

and

$$\|\dot{\mathcal{S}}_{n_L=r_L+1}\|_F = \dots = \|\dot{\mathcal{S}}_{n_L=N_L}\|_F = 0. \quad (15)$$

Consequently, for any quaternion tensor $\dot{\mathcal{T}} \in \mathbb{H}^{N_1 \times N_2 \times \dots \times N_L}$, we can always find unitary quaternion matrices $\dot{\mathbf{U}}_l \in \mathbb{H}^{N_l \times N_l}$ ($l = 1, \dots, L$) and a corresponding quaternion tensor $\dot{\mathcal{S}}$ with the property (4) such that equation (3) holds. The proof is completed.

Based on **Theorem 1**, we can define the following QHOSVD.

Definition 4. (QHOSVD) For an L th-order quaternion tensor $\dot{\mathcal{T}} \in \mathbb{H}^{N_1 \times N_2 \times \dots \times N_L}$, its QHOSVD is defined by

$$\dot{\mathcal{T}} = \dot{\mathcal{S}} \times_1 \dot{\mathbf{U}}_1 \times_2 \dot{\mathbf{U}}_2 \dots \times_L \dot{\mathbf{U}}_L, \quad (16)$$

where $\dot{\mathbf{U}}_l \in \mathbb{H}^{N_l \times N_l}$ ($l = 1, \dots, L$) are unitary quaternion matrices, $\dot{\mathcal{S}} \in \mathbb{H}^{N_1 \times N_2 \times \dots \times N_L}$ is a quaternion tensor with the property

$$\|\dot{\mathcal{S}}_{n_l=1}\|_F \geq \|\dot{\mathcal{S}}_{n_l=2}\|_F \geq \dots \geq \|\dot{\mathcal{S}}_{n_l=N_l}\|_F \geq 0$$

for all possible values of l . The Frobenius-norms $\|\dot{\mathcal{S}}_{n_l=n}\|_F$, labeled by $\sigma_n^{(l)}$, are l th-mode singular values of $\dot{\mathcal{T}}$ and the vector $\dot{\mathbf{U}}_l(:, n)$ is an n th l -mode singular vector. The decomposition is visualized for third-order quaternion tensors in Fig. 1.

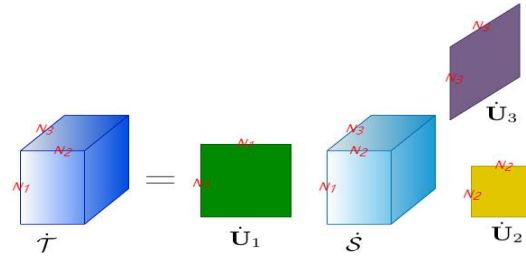


Fig. 1. Visualization of the QHOSVD for a third-order quaternion tensor.

Remark 1. The proof procedure of **Theorem 1** actually indicates how the QHOSVD of a given quaternion tensor $\dot{\mathcal{T}}$ can be computed, which is summarized in Table I.

Remark 2. The fact **4** determines that the calculation procedure of QHOSVD is different from that of HOSVD proposed in [1]. Another difference from HOSVD is that our definition of QHOSVD does not require $\dot{\mathcal{S}}$ to be all-orthogonality⁴. The first reason is that it is quite difficult for the quaternion tensor $\dot{\mathcal{S}}$ to satisfy the same all-orthogonality as that of the real-valued

⁴All-orthogonality for real-valued tensor $\mathcal{S} \in \mathbb{R}^{N_1 \times N_2 \times \dots \times N_L}$ [1]: two sub-tensors $\mathcal{S}_{n_l=\alpha}$ and $\mathcal{S}_{n_l=\beta}$ for all possible values of l , α and β satisfy $\langle \mathcal{S}_{n_l=\alpha}, \mathcal{S}_{n_l=\beta} \rangle = 0$ when $\alpha \neq \beta$.

TABLE I
THE CALCULATION PROCEDURE OF QHOSVD

Input: Quaternion tensor $\hat{\mathcal{T}} \in \mathbb{H}^{N_1 \times N_2 \times \dots \times N_L}$.
1: $\hat{\mathbf{U}}_L \leftarrow$ left singular vectors of $\text{Unfold}_L(\hat{\mathcal{T}})$.
2: **for** $l = (L-1) : -1 : 1$ **do**
3: $\hat{\mathbf{U}}_l \leftarrow$ left singular vectors of $\text{Unfold}_l(\hat{\mathcal{T}} \times_L \hat{\mathbf{U}}_L \dots \times_{l+1} \hat{\mathbf{U}}_{l+1})$.
4: **end for**
5: $\hat{\mathcal{S}} \leftarrow \hat{\mathcal{T}} \times_L \hat{\mathbf{U}}_L^H \times_{L-1} \hat{\mathbf{U}}_{L-1}^H \dots \times_1 \hat{\mathbf{U}}_1^H$.
Output: $\hat{\mathcal{S}}, \{\hat{\mathbf{U}}_1, \hat{\mathbf{U}}_2, \dots, \hat{\mathbf{U}}_L\}$.

tensor in [1]. The orthogonality is satisfied only when $l = 1$ for the obtained $\hat{\mathcal{S}}$. Since comparing (9) and (10), we can find that $\hat{\mathcal{S}}_{[1]} = \Sigma_1 \hat{\mathbf{V}}_1^H$, where $\hat{\mathbf{V}}_1^H$ is unitary, which means $\langle \hat{\mathcal{S}}_{n_1=\alpha}, \hat{\mathcal{S}}_{n_1=\beta} \rangle = 0$. However, for other values of l , the orthogonality is generally not satisfied. From equation (12), for example, we can find that $(\hat{\mathbf{V}}_L^T (\hat{\mathbf{U}}_{L-1} \otimes \dots \otimes \hat{\mathbf{U}}_1))^*$ is generally no longer a unitary matrix since $\hat{\mathbf{V}}_L^T$ is generally no longer unitary (see **Theorem 1** (d)), which means that generally $\langle \hat{\mathcal{S}}_{n_L=\alpha}, \hat{\mathcal{S}}_{n_L=\beta} \rangle \neq 0$, the same is true for all the other values of l except $l = 1$. The second reason is that the definition of QHOSVD in this paper is application-oriented. In practice, it is irrelevant whether $\hat{\mathcal{S}}$ is all-orthogonality or not in the considered applications.

V. APPLICATIONS OF QHOSVD IN COLOR IMAGE PROCESSING

In this section, based on the defined QHOSVD, we develop a multi-focus color image fusion method and a color image denoising method. In these methods, each color pixel with R, G, B channels is encoded as a pure quaternion unit. That is

$$\hat{a} = a_r i + a_g j + a_b k, \quad (17)$$

where \hat{a} denotes a color pixel, the coefficients a_r, a_g, a_b of the imaginary parts are respectively the pixel values in R, G, B channels. Naturally, a given color image with the spatial resolution of $N_1 \times N_2$ pixels can be represented by a pure quaternion matrix $\hat{\mathbf{A}} = (\hat{a}_{n_1 n_2}) \in \mathbb{H}^{N_1 \times N_2}$, $1 \leq n_1 \leq N_1, 1 \leq n_2 \leq N_2$ as follows:

$$\hat{\mathbf{A}} = \mathbf{A}_r i + \mathbf{A}_g j + \mathbf{A}_b k, \quad (18)$$

where $\mathbf{A}_r, \mathbf{A}_g, \mathbf{A}_b \in \mathbb{R}^{N_1 \times N_2}$ containing respectively R, G, B pixel values. Fig. 2 shows an example of using a quaternion matrix to represent a color image.

From (18), we can see that, based on the quaternion representation, when we process the color image $\hat{\mathbf{A}}$, the three RGB channels can be handled holistically. Thus, the high correlation among RGB channels can be fully utilized. Different from the real third-order

$$\hat{\mathbf{A}} = \mathbf{A}_r i + \mathbf{A}_g j + \mathbf{A}_b k$$

Fig. 2. Quaternion matrix represented color image.

tensor representation, the quaternion matrix is still a two-dimensional array, which has no dimension increase and is easy to calculate and process.

A. Multi-focus color image fusion using QHOSVD

Multi-focus color image fusion is to create an all-focus color image from a set of partially focused color images of the same scene. Since these partially focused color images refer to the same scene and are highly similar, we construct them (represented as quaternion matrices) into a third-order quaternion tensor and adopt the proposed QHOSVD technique to extract their features simultaneously.

The whole framework of the proposed multi-focus color image fusion method is shown in Fig. 3. We, in the following, show the detailed procedure of the proposed method step by step.

Step 1: All the partially focused color images are represented by pure quaternion matrices $\hat{\mathbf{A}}_1, \hat{\mathbf{A}}_2, \dots, \hat{\mathbf{A}}_K \in \mathbb{H}^{N_1 \times N_2}$. Then, the sliding window technique is applied to divide each source color image $\hat{\mathbf{A}}_k, (k = 1, \dots, K)$ into D overlapping patches $\hat{\mathbf{P}}_k^d \in \mathbb{H}^{M_1 \times M_2}, (d = 1, \dots, D)$. Afterwards, for each d , all of the patches from K source color images are stacked together to form a third-order quaternion tensor $\hat{\mathcal{T}}_d \in \mathbb{H}^{M_1 \times M_2 \times K}, (d = 1, \dots, D)$.

Step 2: Using QHOSVD procedure on $\hat{\mathcal{T}}_d$ to find two unitary matrices $\hat{\mathbf{U}}_1^d \in \mathbb{H}^{M_1 \times M_1}$ and $\hat{\mathbf{U}}_2^d \in \mathbb{H}^{M_2 \times M_2}$, and the corresponding third-order quaternion tensor $\hat{\mathcal{S}}_d \in \mathbb{H}^{M_1 \times M_2 \times K}$ such that

$$\hat{\mathcal{T}}_d = \hat{\mathcal{S}}_d \times_1 \hat{\mathbf{U}}_1^d \times_2 \hat{\mathbf{U}}_2^d. \quad (19)$$

Remark 3. It can be found that in (19) we do not perform a complete QHOSVD procedure (i.e., there is no $\hat{\mathbf{U}}_3^d$ in (19)), which is different from the traditional HOSVD-based methods [2], [29]. The reasons are listed below.

- (a) In (19), $\hat{\mathcal{S}}_d$ is the coefficient tensor, and generally can be seen as the feature of $\hat{\mathcal{T}}_d$. Our goal is to find the features corresponding to each source color

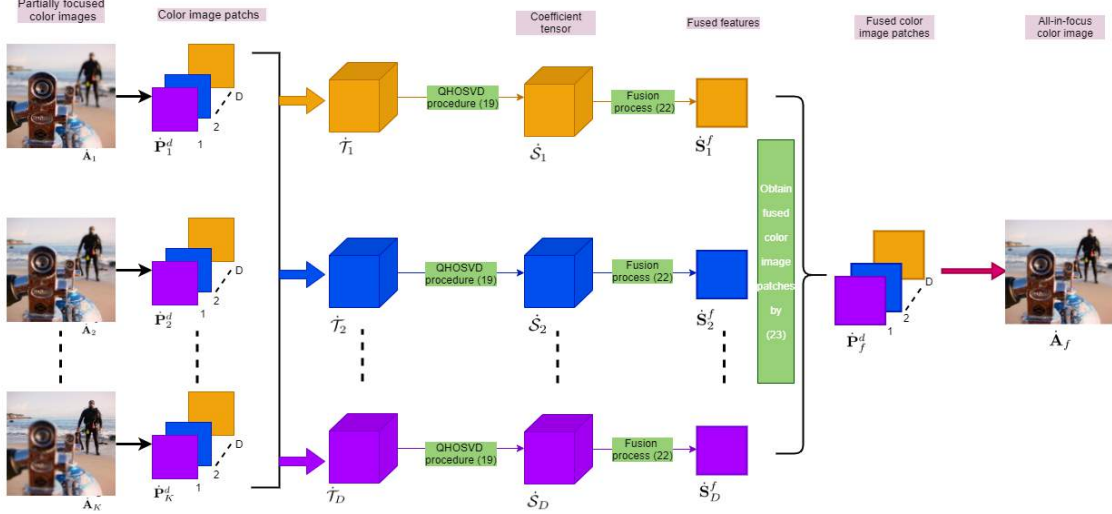


Fig. 3. The flowchart of multi-focus color image fusion by QHOSVD.

image patch $\tilde{\mathcal{T}}_d(:, :, k)$, ($k = 1, \dots, K$). After a simple but important derivation, we can find that

$$\tilde{\mathcal{T}}_d(:, :, k) = \left(\tilde{\mathbf{U}}_2^d (\tilde{\mathbf{U}}_1^d \hat{\mathcal{S}}_d(:, :, k))^T \right)^T, \quad (20)$$

for $k = 1, \dots, K$.

From (20), $\hat{\mathcal{S}}_d(:, :, k)$ can be seen as the feature of source color image patch $\tilde{\mathcal{T}}_d(:, :, k)$, for $k = 1, \dots, K$. Because for all $\hat{\mathcal{S}}_d(:, :, k)$ ($k = 1, \dots, K$), they share the common $\tilde{\mathbf{U}}_1$ and $\tilde{\mathbf{U}}_2$, the features are extracted simultaneously.

- (b) If we perform a complete QHOSVD procedure on $\tilde{\mathcal{T}}_d$, i.e.,

$$\tilde{\mathcal{T}}_d = \tilde{\mathcal{S}}_d \times_1 \tilde{\mathbf{U}}_1^d \times_2 \tilde{\mathbf{U}}_2^d \times_3 \tilde{\mathbf{U}}_3^d, \quad (21)$$

it will be pretty difficult to find the corresponding features of each source color image patch $\tilde{\mathcal{T}}_d(:, :, k)$, ($k = 1, \dots, K$). Since, based on the fact ❸, generally $\tilde{\mathcal{S}}_d \times_3 \tilde{\mathbf{U}}_3^d \neq \hat{\mathcal{S}}_d$, which is different from real-valued HOSVD procedure [1].

- (c) The traditional HOSVD-based methods [2], [29] are to make a complete HOSVD procedure first, and then multiply the third mode of the obtained feature tensor by the corresponding third singular vector matrix, to obtain a new feature tensor. Even if we could do the same process, it would be redundant and not conducive to saving calculation costs.

Step 3: To fuse features $\hat{\mathcal{S}}_d(:, :, k)$, ($k = 1, \dots, K$) by the following way:

$$\hat{\mathcal{S}}_d^f = \hat{\mathcal{S}}_d(:, :, \xi), \quad (22)$$

in which the index ξ satisfies

$$\|\hat{\mathcal{S}}_d(:, :, \xi)\|_{L_1} = \max_{k \in (1, 2, \dots, K)} \{\|\hat{\mathcal{S}}_d(:, :, k)\|_{L_1}\}.$$

Or $\hat{\mathcal{S}}_d^f = (\hat{\mathcal{S}}_d(:, :, 1) + \dots + \hat{\mathcal{S}}_d(:, :, K))/K$, if $\|\hat{\mathcal{S}}_d(:, :, 1)\|_{L_1} = \dots = \|\hat{\mathcal{S}}_d(:, :, K)\|_{L_1}$.

Step 4: The fused color image patch $\hat{\mathbf{P}}_f^d$ is obtained by:

$$\hat{\mathbf{P}}_f^d = \left(\tilde{\mathbf{U}}_2^d (\tilde{\mathbf{U}}_1^d \hat{\mathcal{S}}_d^f)^T \right)^T. \quad (23)$$

Step 5: Take all the fused color image patches $\hat{\mathbf{P}}_f^d$, ($d = 1, \dots, D$) back to their original corresponding positions. The final fused color image $\hat{\mathbf{A}}_f$ is reconstructed by averaging the overlapping fused color image patches.

B. Color image denoising using QHOSVD

Color image denoising is to recover the clear image $\hat{\mathbf{X}} \in \mathbb{H}^{M \times N}$ from its noisy observation

$$\hat{\mathbf{Y}} = \hat{\mathbf{X}} + \hat{\mathbf{G}}, \quad (24)$$

where $\hat{\mathbf{G}}$ is assumed to be Gaussian noise. The recent quaternion matrix low-rank approximation-based color image denoising methods proposed in [8], [9] are also based on the above observation model (24). And the NNS which has significantly boosted the performance of image denoising is adopted in these works. However, these methods may destroy the two-dimensional structure information of color image patches when they are expanded into one-dimensional quaternion vectors. To avoid pulling color image patches into one-dimensional

quaternion vectors, similar image patches are stacked into a third-order quaternion tensor, and then the proposed QHOSVD can be performed on it. The detailed procedure of color image denoising is listed below.

Firstly, using the sliding window technique, the noisy color image represented by pure quaternion matrix $\hat{\mathbf{Y}}$ is divided into overlapped patches $\hat{\mathbf{P}}_i \in \mathbb{H}^{w \times w}$. The j th reference patch $\hat{\mathbf{P}}_{ref}^j \in \mathbb{H}^{w \times w}$ is taken as the center of the searching window with size $W \times W$. For each reference patch $\hat{\mathbf{P}}_{ref}^j$, search for K similar patches (including the reference patch itself) within its local searching window. The similarity is determined by the following distance:

$$d(\hat{\mathbf{P}}_{ref}^j, \hat{\mathbf{P}}_i) = \|\hat{\mathbf{P}}_{ref}^j - \hat{\mathbf{P}}_i\|_F^2.$$

At last, for each reference patch $\hat{\mathbf{P}}_{ref}^j$, its K similar patches are stacked together to form a third-order quaternion tensor $\hat{\mathcal{Y}}_j \in \mathbb{H}^{w \times w \times K}$. It should be noted that this step is different from that in [8] and [9], in which the K similar patches are first expanded into one-dimensional quaternion vectors which then construct a quaternion matrix with size $w^2 \times K$. Such operations may destroy the two-dimensional spatial structure of color image patches and may lead to the curse of dimensionality.

Following (24), each third-order quaternion tensor $\hat{\mathcal{Y}}_j$ has the following form:

$$\hat{\mathcal{Y}}_j = \hat{\mathcal{X}}_j + \hat{\mathcal{G}}_j, \quad (25)$$

where, $\hat{\mathcal{X}}_j \in \mathbb{H}^{w \times w \times K}$ is the quaternion tensor stacked by clear color image patches, which is what we need to estimate, and $\hat{\mathcal{G}}_j \in \mathbb{H}^{w \times w \times K}$ is the corresponding noise part. Then, we perform the QHOSVD procedure on $\hat{\mathcal{Y}}_j$, *i.e.*,

$$(\hat{\mathcal{S}}_j, \{\hat{\mathbf{U}}_1^j, \hat{\mathbf{U}}_2^j, \hat{\mathbf{U}}_3^j\}) = QHOSVD(\hat{\mathcal{Y}}_j). \quad (26)$$

The third-mode (similar to other modes) singular values of $\hat{\mathcal{Y}}_j$ are

$$\sigma_k^{(3)} = \|\hat{\mathcal{S}}_j(:, :, k)\|_F, \quad k = 1, 2, \dots, K. \quad (27)$$

From the formula (27), we can see that the coefficients in $\hat{\mathcal{S}}_j$ are actually to re-decompose the corresponding singular values so that the noise energy originally concentrated on the singular values is mainly transferred to the smaller coefficients in $\hat{\mathcal{S}}_j$ while larger coefficients are less affected by noise [5]. Thus, to perform denoising, the smaller coefficients are truncated by adopting the following method of hard threshold shrinkage:

$$\hat{\mathcal{S}}_j = \text{Hard}(\hat{\mathcal{S}}_j, \tau), \quad (28)$$

where $\text{Hard}(*, \tau)$ is defined as

$$\text{Hard}(*, \tau) = \begin{cases} *, & \text{if } |*| \geq \tau, \\ 0, & \text{otherwise,} \end{cases} \quad (29)$$

and τ is chosen to be $\eta\sigma\sqrt{2\log(\omega^2K)}$ (in which, σ stands for the standard deviation of the noise, η is a scale that controls the smoothing degree in the denoising stage, $\sigma\sqrt{2\log(\omega^2K)}$ is the optimal threshold from a statistical risk viewpoint [34]).

Afterwards, the denoised quaternion tensor $\hat{\mathcal{X}}_j$ (*i.e.*, the estimated $\hat{\mathcal{X}}_j$) can be obtained by inverse QHOSVD:

$$\hat{\mathcal{X}}_j = \hat{\mathcal{S}}_j \times_1 \hat{\mathbf{U}}_1^j \times_2 \hat{\mathbf{U}}_2^j \times_3 \hat{\mathbf{U}}_3^j. \quad (30)$$

That means the denoised K similar patches corresponding to the reference patch $\hat{\mathbf{P}}_{ref}^j$ are obtained. Then, put all the denoised patches back to the original position of the color image. The final denoised color image $\hat{\mathbf{X}}$ (*i.e.*, the estimated $\hat{\mathbf{X}}$) is reconstructed by averaging all the overlapping color image patches together. And the iterative regularization scheme [8], [9], [35], *etc.*, is adopted

$$\hat{\mathbf{Y}}^{(\gamma)} = \hat{\mathbf{X}}^{(\gamma-1)} + \delta(\hat{\mathbf{Y}} - \hat{\mathbf{X}}^{(\gamma-1)}),$$

where γ and δ are respectively the iteration number and the relaxation parameter.

The flowchart of QHOSVD for color image denoising is shown in Fig. 4. The whole denoising algorithm can be summarized in Table II.

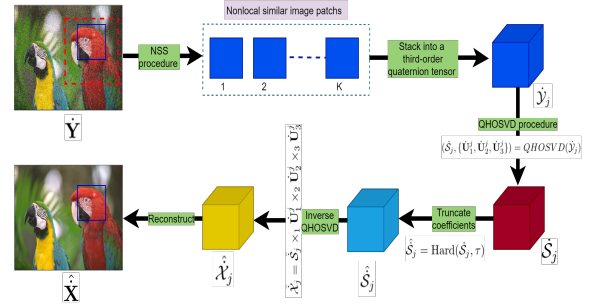


Fig. 4. The flowchart of color image denoising by QHOSVD.

VI. EXPERIMENTAL RESULTS

In this section, several experiments are conducted to evaluate the effectiveness of the proposed QHOSVD-based multi-focus color image fusion method and color image denoising method. All the experiments are run in MATLAB 2014b (except for one of the multi-focus color image fusion methods: MADCNN, which is performed in Python) under Windows 10 on a personal computer with a 1.60GHz CPU and 8GB memory.

TABLE II
COLOR IMAGE DENOISING BY QHOSVD.

Input: The observed noisy color image represented by a quaternion matrix $\hat{\mathbf{Y}}$, regularization parameter δ , search window size $W \times W$, patch size $\omega \times \omega$, similar patch number K , iteration number \mathcal{T} .

- 1: **Initialize** $\hat{\mathbf{X}}^{(0)} = \hat{\mathbf{Y}}$, $\hat{\mathbf{Y}}^{(0)} = \hat{\mathbf{Y}}$.
- 2: **for** $\gamma = 1 : \mathcal{T}$ **do**
- 3: Iterative regularization $\hat{\mathbf{Y}}^{(\gamma)} = \hat{\mathbf{X}}^{(\gamma-1)} + \delta(\hat{\mathbf{Y}} - \hat{\mathbf{X}}^{(\gamma-1)})$
- 4: **for** each reference patch $\hat{\mathbf{P}}_{ref}^j$ in $\hat{\mathbf{Y}}^{(i)}$ **do**
- 5: Find K similar patches, and stack into a third-order quaternion tensor $\hat{\mathcal{Y}}_j \in \mathbb{H}^{\omega \times \omega \times K}$.
- 6: Perform the QHOSVD on $\hat{\mathcal{Y}}_j$: $(\hat{\mathcal{S}}_j, \{\hat{\mathbf{U}}_1^j, \hat{\mathbf{U}}_2^j, \hat{\mathbf{U}}_3^j\}) = QHOSVD(\hat{\mathcal{Y}}_j)$.
- 7: Truncate the coefficients $\hat{\mathcal{S}}_j$: $\hat{\mathcal{S}}_j = \text{Hard}(\hat{\mathcal{S}}_j, \tau)$.
- 8: Perform the inverse QHOSVD on $\hat{\mathcal{S}}_j$: $\hat{\mathcal{X}}_j = \hat{\mathcal{S}}_j \times_1 \hat{\mathbf{U}}_1^j \times_2 \hat{\mathbf{U}}_2^j \times_3 \hat{\mathbf{U}}_3^j$.
- 9: **end for**
- 10: Compute the average of repeated estimates for every patch, and aggregate all patches together, get the clean image $\hat{\mathbf{X}}^{(\gamma)}$.
- 11: **end for**

Output: Denoised color image $\hat{\mathbf{X}}^{(\mathcal{T})}$.

A. Multi-focus color image fusion

Dataset: We conduct the experiments on a popular multi-focus image dataset, Lytro [36], which is publicly available online⁵. The 20 pairs (with two images) of color multi-focus images of size 520×520 pixels are adopted from the dataset. They are shown in Fig. 5.



Fig. 5. The used multi-focus color images in our experiments.

Objective metrics: In our experiments, six metrics that are widely used in multi-focus image fusion are adopted for evaluation and are listed below.

- Information theory-based: Normalized mutual information Q_{MI} [37] and Nonlinear correlation information entropy Q_{NCIE} [38], which measure the amount of mutual information between the fused image and the source images.
- Image feature-based: Multiscale scheme based Q_M [39], which measures the extent of edge information injected into the fused image from the source images.

⁵<https://mansournejati.ece.iut.ac.ir/content/lytro-multi-focus-dataset>.

- Image structural similarity-based: Q_Y [39], which measures the amount of structural information preserved in the fused image.
- Human perception-based: Q_{CB} [40] and Q_{CV} [41], which address the major features in the human visual system.

For all metrics except Q_{CV} , a larger value indicates a better fusion performance [14], [42].

Methods for comparison: We compare our QHOSVD-based method with several representative methods including traditional ones and latest ones. Specifically, they are transform domain methods: DWT [15], NSCT [16], MWGF [17], GFF [18], QCT [28], HOSVD [2]; spatial domain methods: QUADTREE [19], GFDF [20], MISF [21]; deep learning methods: CNN [22], MADCNN [23].

Parameter setting: For our method, the size of each patch is empirically set as $M_1 = M_2 = 25$, and the patches are overlapped with 6 pixels. All compared methods are from the source codes, and the parameter settings are based on the suggestions in the original papers.

TABLE III
THE AVERAGE SCORES OF DIFFERENT FUSION METHODS (**BOLD** FONTS DENOTE THE BEST PERFORMANCE; UNDERLINE ONES REPRESENT THE SECOND-BEST RESULTS).

Methods	Metrics						Time(s)
	Q_{MI}	Q_{NCIE}	Q_M	Q_Y	Q_{CB}	Q_{CV}	
DWT [15]	0.8389	0.8254	2.9091	0.9249	0.6232	67.5382	0.2890
NSCT [16]	0.9284	0.8301	2.9692	0.9646	0.6953	22.5183	14.1024
MWGF [17]	1.1076	0.8422	2.8991	0.9863	0.8036	19.3433	7.4339
GFF [18]	1.0755	0.8395	2.9688	0.9820	0.7981	16.4563	1.1895
QCT [28]	0.8970	0.8285	2.9622	0.9453	0.6214	43.3072	97.1247
HOSVD [2]	1.1299	0.8431	2.9690	0.9813	0.8050	18.6918	5.0940
QUADTREE [19]	0.8639	0.8269	2.8385	0.8643	0.6197	49.9656	1.3634
GFDF [20]	1.1431	<u>0.8440</u>	2.9712	0.9870	0.8145	16.8288	0.3519
MISF [21]	1.1359	0.8435	2.9693	0.9860	0.8114	20.7648	0.4688
CNN [22]	1.1305	0.8432	2.9710	<u>0.9871</u>	<u>0.8118</u>	16.7943	209.6695
MADCNN [23]	<u>1.1421</u>	0.8439	2.9717	0.9858	0.8078	<u>16.7676</u>	\
QHOSVD	1.1465	0.8441	<u>2.9715</u>	0.9874	0.8093	17.6980	7.8943

Results and discussions: Fig. 6 provides insights about the objective performance of different fusion methods on the 20 pairs of color multi-focus images. TABLE III lists the objective performance (average score of each metric) and average running time of different fusion methods. Fig. 7 visually shows one of the fusion results of different methods. From all the experimental results about multi-focus color image fusion, we can observe and summarize the following points.

- The defined QHOSVD can indeed be applied to multi-focus color image fusion problems.

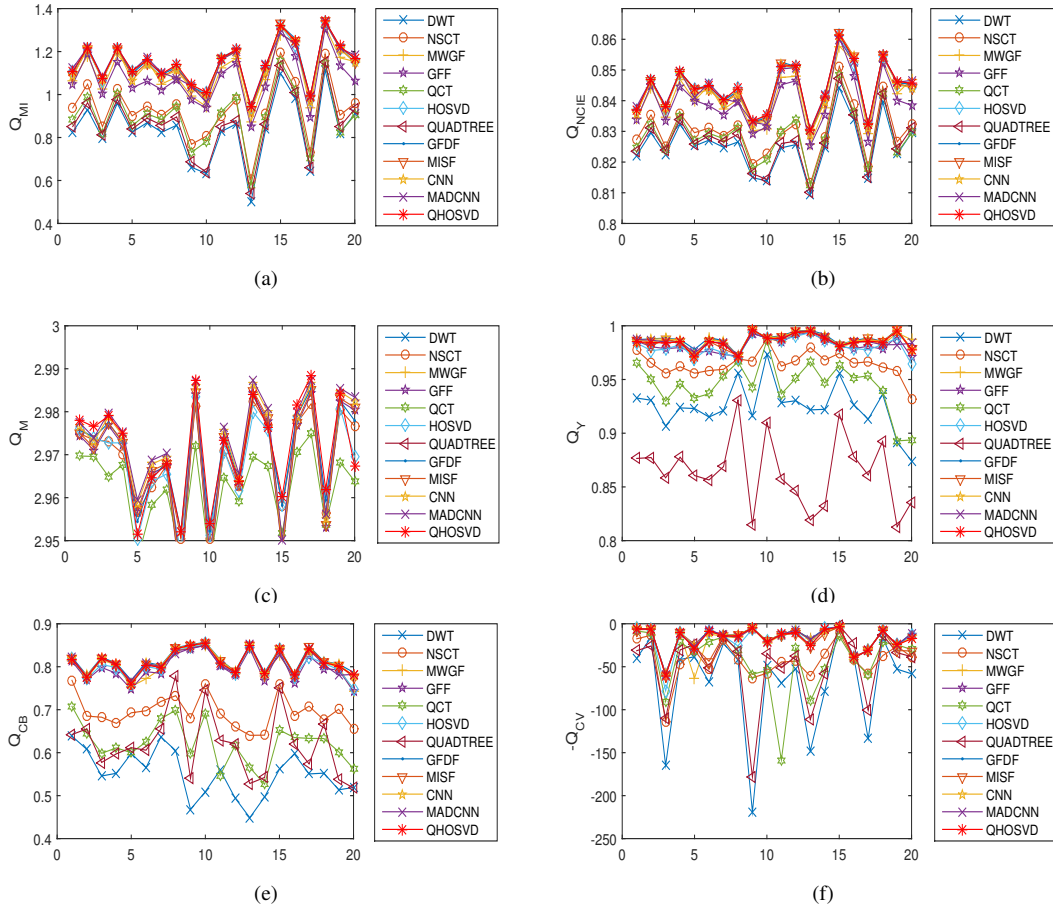


Fig. 6. Objective performance of different fusion methods on the 20 pairs of color multi-focus images (the figure is viewed better in zoomed PDF).

- Compared with the traditional fusion methods (e.g., DWT, NSCT, MWGF, GFF, QCT, HOSVD, and QUADTREE), the proposed QHOSVD-based method has great advantages. Compared with the latest fusion methods (e.g., GFDF and MISF) and even methods based on deep learning (e.g., CNN and MADCNN), our method still has a small advantage on Q_{MI} , Q_{NCIE} , and Q_Y . Although our method is not competitive on Q_{CB} and Q_{CV} , they are not far from the best value.
- Except for CNN and QCT, most of the methods only require a few seconds or less one second to accomplish the fusion task. We do not list the running time of MADCNN because its source code is a Python version, we perform it in Python. Therefore, it is not comparable.

B. Color image denoising

Dataset: We conduct the experiments on 10 color images with size 121×181 shown in Fig. 8. The 5 images in the first row are randomly selected from the Berkeley Segmentation Dataset (BSD)⁶. The second row is the most widely used 5 images in digital image processing.

Objective metrics: To evaluate the performance of proposed methods, except visual quality, we employ two widely used quantitative quality indexes, including the peak signal-to-noise ratio (PSNR) and the structure similarity (SSIM) [43]. For both metrics, a larger value indicates a better denoising performance.

Methods for comparison: We compare our QHOSVD-based method with four state-of-the-art denoising methods including QNNM [8] (a quaternion nuclear norm minimization algorithm labeled as LRQA-1 in [8]), QWNNM [9] (a quaternion weighted nuclear

⁶<https://www2.eecs.berkeley.edu/Research/Projects/CS/vision/bsds/>.

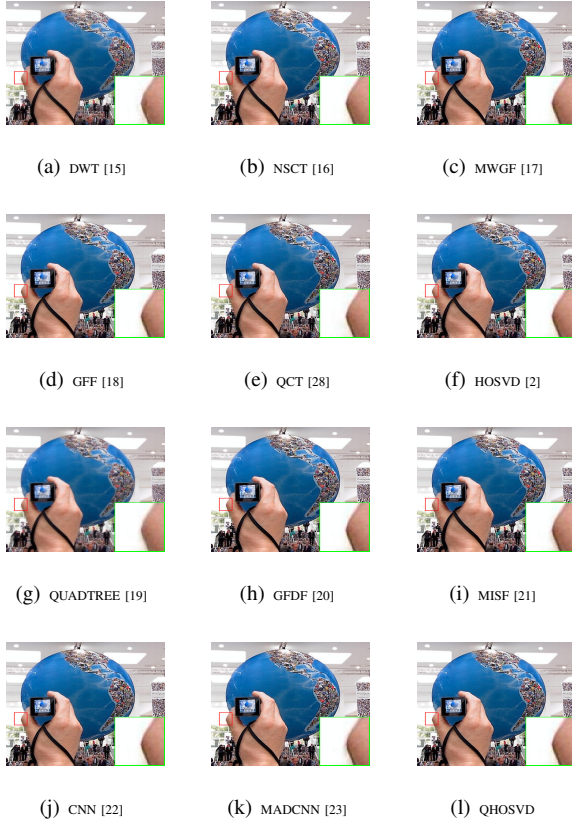


Fig. 7. The fusion results on the 11th pair with detail magnified for all methods.

norm minimization algorithm), LRQA-WSNN [8] (a quaternion weighted Schatten norm minimization algorithm labeled as LRQA-4 in [8]), and HOSVD-based method [5].

Parameter setting: For the NSS procedure, the same parameters are set for all methods. Specifically, when $\delta = 10, 20, 30, 50$, the patch size is set to 6×6 , 6×6 , 7×7 , and 8×8 , respectively. The number of similar patches K is set to 70, 70, 90, and 120, respectively. The iteration \mathcal{Y} is set to 8, 8, 14, and 20, respectively. For all noise levels, the iterative relaxation parameter δ is fixed to 0.1, and the searching window size is fixed to 30×30 . For our QHOSVD-based method, η is empirically set to 0.70, 0.55, 0.45, and 0.35, respectively. In addition, all compared methods are from the source codes and the parameter settings are based on the suggestions in the original papers.

Results and discussions: TABLE IV reports the quantitative PSNR and SSIM values (and the average values of them) of all denoising methods on the ten testing color images with different noise level. Fig. 9-



Fig. 8. The 10 color images for color image denoising in our experiments (Image(1)-Image(10) from left to right, top to bottom).

TABLE IV
OBJECTIVE METRICS (PSNR/SSIM) OF DIFFERENT METHODS ON THE TEN COLOR IMAGES (**BOLD** FONTS DENOTE THE BEST PERFORMANCE; UNDERLINE ONES REPRESENT THE SECOND-BEST RESULTS).

Methods:	QNNM [8]	QWNNM [9]	LRQA-WSNN [8]	HOSVD [5]	QHOSVD
Images: $\sigma = 10$					
Image(1)	35.234/0.952	<u>35.881/0.966</u>	35.800/0.966	35.496/0.961	35.895/0.967
Image(2)	31.113/0.975	31.356/0.978	<u>31.371/0.979</u>	31.240/0.977	31.373/0.978
Image(3)	32.624/0.975	<u>33.138/0.980</u>	33.123/0.980	32.682/0.977	33.337/0.982
Image(4)	36.117/0.992	37.330/0.994	<u>37.358/0.993</u>	36.550/0.993	37.472/0.995
Image(5)	32.915/0.981	33.767/0.983	<u>33.803/0.983</u>	33.134/0.980	33.814/0.984
Image(6)	31.735/0.987	32.873/0.991	32.682/0.990	32.388/0.989	33.024/0.991
Image(7)	32.937/0.990	34.069/0.992	<u>34.116/0.992</u>	33.805/0.992	34.094/0.993
Image(8)	30.743/0.948	30.866/0.951	<u>30.881/0.952</u>	30.603/0.945	31.044/0.954
Image(9)	34.512/0.969	<u>35.444/0.976</u>	35.366/0.974	35.044/0.975	35.454/0.977
Image(10)	33.613/0.990	34.443/0.991	<u>34.530/0.991</u>	33.900/0.990	34.604/0.992
Aver.	33.154/0.976	<u>33.917/0.980</u>	33.903/0.980	33.484/0.977	34.011/0.981
Images: $\sigma = 20$					
Image(1)	31.904/0.907	<u>32.312/0.926</u>	32.218/0.925	32.014/0.923	32.326/0.927
Image(2)	27.311/0.931	27.585/0.952	<u>27.801/0.954</u>	27.592/0.953	27.914/0.954
Image(3)	29.099/0.930	29.630/0.952	<u>29.715/0.954</u>	29.042/0.949	29.794/0.958
Image(4)	31.926/0.978	33.693/0.988	<u>33.682/0.987</u>	32.389/0.983	33.624/0.988
Image(5)	29.293/0.949	29.984/0.964	<u>30.012/0.964</u>	29.671/0.963	30.023/0.966
Image(6)	27.267/0.947	28.668/0.975	<u>28.709/0.975</u>	28.217/0.902	28.753/0.976
Image(7)	29.062/0.968	<u>30.144/0.982</u>	30.115/0.982	29.891/0.981	30.151/0.983
Image(8)	27.049/0.815	27.449/0.886	<u>27.513/0.876</u>	27.171/0.883	27.574/0.888
Image(9)	30.917/0.931	31.819/0.952	<u>31.844/0.953</u>	31.242/0.948	31.884/0.954
Image(10)	30.034/0.969	30.846/0.982	<u>30.901/0.981</u>	30.093/0.978	30.914/0.983
Aver.	29.386/0.933	30.213/0.956	<u>30.251/0.955</u>	29.732/0.946	30.296/0.958
Images: $\sigma = 30$					
Image(1)	28.747/0.864	<u>30.351/0.896</u>	30.181/0.895	30.064/0.892	30.534/0.899
Image(2)	25.201/0.908	25.633/0.933	<u>25.793/0.935</u>	25.504/0.930	25.900/0.936
Image(3)	26.645/0.903	27.567/0.929	<u>27.638/0.930</u>	27.073/0.924	27.644/0.931
Image(4)	27.939/0.957	<u>30.929/0.977</u>	30.918/0.976	29.486/0.969	30.944/0.979
Image(5)	26.626/0.921	27.818/0.941	<u>27.820/0.942</u>	27.714/0.940	27.848/0.943
Image(6)	24.816/0.912	26.129/0.957	<u>26.202/0.957</u>	25.339/0.950	26.217/0.961
Image(7)	26.302/0.952	<u>27.772/0.970</u>	27.737/0.967	27.540/0.969	27.803/0.971
Image(8)	25.335/0.778	25.694/0.822	<u>25.726/0.834</u>	25.481/0.834	25.774/0.845
Image(9)	27.651/0.897	29.447/0.922	<u>29.529/0.924</u>	28.979/0.919	29.615/0.931
Image(10)	27.158/0.957	28.785/0.971	<u>28.790/0.971</u>	27.982/0.965	28.798/0.974
Aver.	26.739/0.905	28.013/0.932	<u>28.033/0.933</u>	27.516/0.921	28.189/0.937
Images: $\sigma = 50$					
Image(1)	27.198/0.815	23.262/0.714	27.959/0.855	<u>28.110/0.856</u>	28.180/0.861
Image(2)	22.753/0.835	23.498/0.895	<u>23.525/0.889</u>	23.319/0.895	23.534/0.898
Image(3)	24.702/0.827	25.229/0.886	<u>25.321/0.890</u>	24.945/0.883	25.394/0.894
Image(4)	25.751/0.891	<u>27.251/0.948</u>	27.201/0.944	26.277/0.937	27.291/0.951
Image(5)	24.438/0.840	25.255/0.900	<u>25.301/0.899</u>	25.221/0.901	25.318/0.906
Image(6)	21.707/0.823	<u>23.208/0.913</u>	23.199/0.915	22.495/0.904	23.234/0.919
Image(7)	23.776/0.893	<u>24.946/0.946</u>	24.915/0.946	24.830/0.945	25.001/0.948
Image(8)	23.452/0.677	23.841/0.773	<u>23.857/0.768</u>	23.742/0.771	23.904/0.786
Image(9)	25.659/0.806	26.768/0.881	<u>26.782/0.880</u>	26.410/0.873	26.984/0.892
Image(10)	25.251/0.921	<u>26.218/0.951</u>	26.206/0.950	25.647/0.945	26.244/0.952
Aver.	24.510/0.833	24.948/0.881	<u>25.427/0.894</u>	25.100/0.891	25.508/0.901

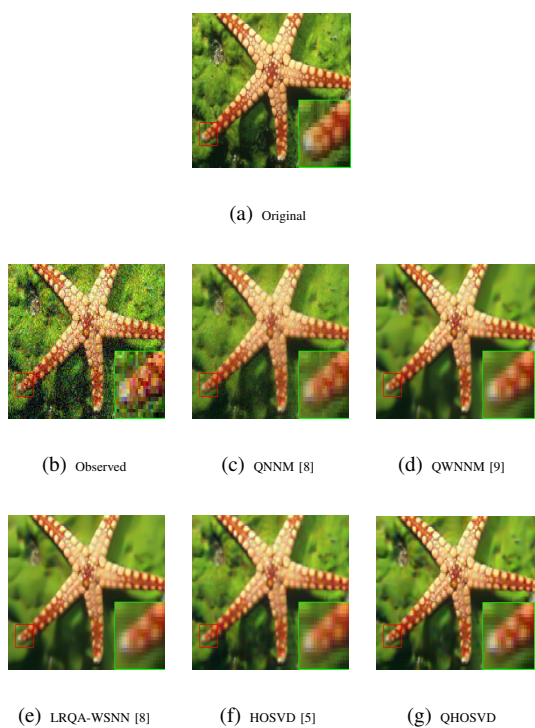


Fig. 9. Color image denoising results on the Image(2) ($\sigma = 20$).

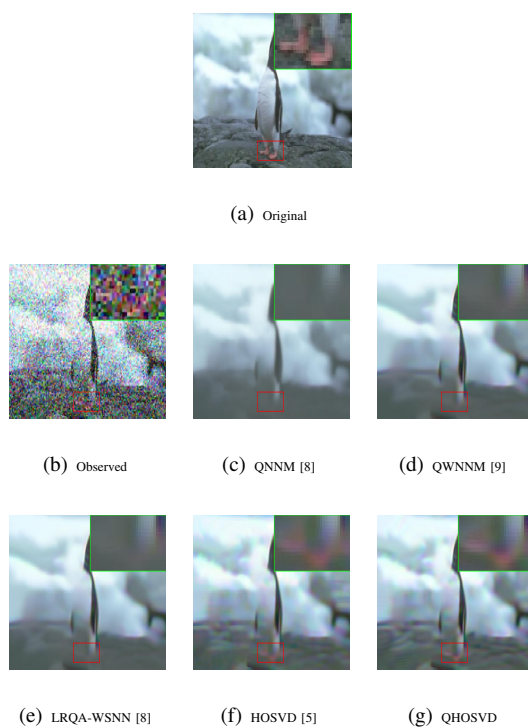


Fig. 11. Color image denoising results on the Image(1) ($\sigma = 50$).

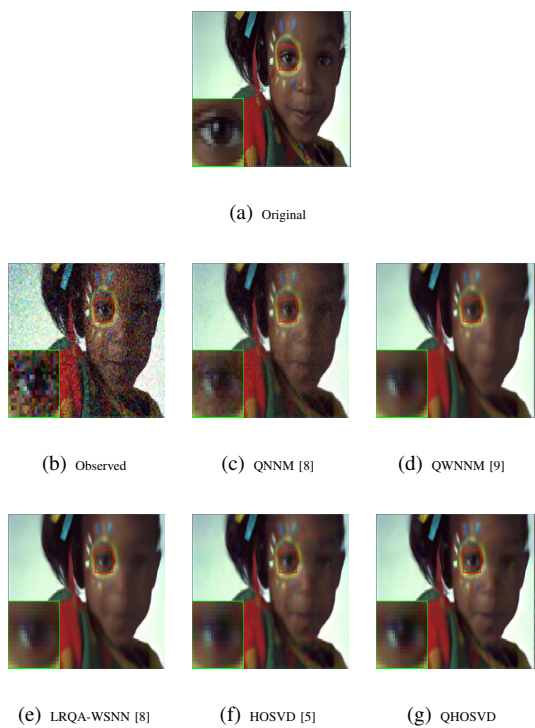


Fig. 10. Color image denoising results on the Image(9) ($\sigma = 20$).

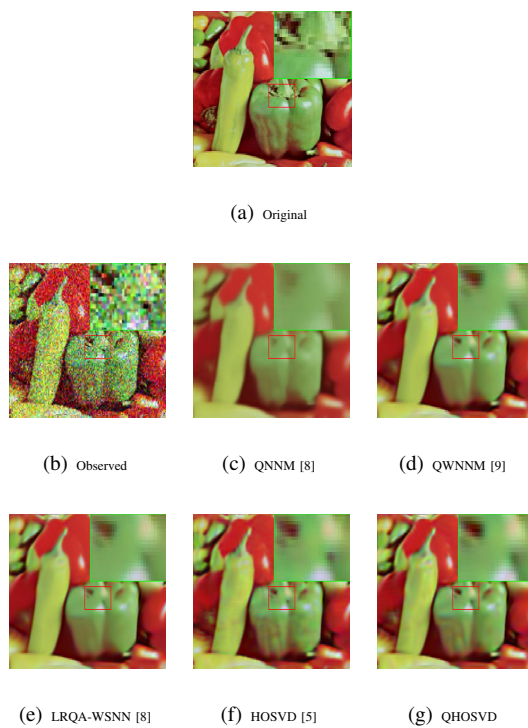


Fig. 12. Color image denoising results on the Image(7) ($\sigma = 50$).

Fig. 12 visually show the denoising results of several color images. From all the experimental results about color image denoising, we can observe and summarize the following points.

- The defined QHOSVD can indeed be applied to color image denoising problems.
- In the overwhelming majority of cases, the proposed QHOSVD-based method shows the best performance among the compared latest ones (see TABLE IV). Visually, the QHOSVD-based method preserves the detail of the color images better, which can notably alleviate the oversmooth problem of QWNNM and LRQA-WSNN (see Fig. 9-Fig. 12).
- The average runtime (when $\sigma = 10$) of QNNM, QWNNM, LRQA-WSNN, HOSVD, and QHOSVD are, 1024.623s, 1036.158s, 1250.813s, 406.486s, and 4065.666s, respectively. The main computation burden of the QHOSVD-based method is performing the QSVD and the NSS procedure, which are generally time-consuming.

VII. CONCLUSION

In this paper, the problem of generalizing the HOSVD to the quaternion domain is investigated. We define QHOSVD and give the calculation procedure. Since the QHOSVD combines the benefits of the quaternion tool and the HOSVD, it can be well applied to many color image processing problems. Moreover, we propose a multi-focus color image fusion method and a color image denoising method, as examples of the QHOSVD in color image processing. Experimental results demonstrate the effectiveness of the developed methods.

Since the computation based on quaternion algebra is still time-consuming, such as the calculation of the QSVD, one of the future works is to study the fast algorithms of the QSVD and other quaternion-based operations to make the proposed QHSVD-based methods more efficient. In addition, we would like to extend the defined QHOSVD to other color image processing tasks, such as color face recognition, color image super-resolution, color image inpainting, and so on.

APPENDIX A

BASIC KNOWLEDGE OF QUATERNION ALGEBRAS

A quaternion $\dot{q} \in \mathbb{H}$ with a real component and three imaginary components is defined as

$$\dot{q} = q_0 + q_1i + q_2j + q_3k, \quad (31)$$

where $q_l \in \mathbb{R}$ ($l = 0, 1, 2, 3$), and i, j, k are imaginary number units and obey the quaternion rules that

$$\begin{cases} i^2 = j^2 = k^2 = ijk = -1, \\ ij = -ji = k, jk = -kj = i, ki = -ik = j. \end{cases} \quad (32)$$

\dot{q} can be decomposed into a real part $\Re(\dot{q}) := q_0$ and an imaginary part $\Im(\dot{q}) := q_1i + q_2j + q_3k$ such that $\dot{q} = \Re(\dot{q}) + \Im(\dot{q})$. If the real part $\Re(\dot{q}) = 0$, \dot{q} is named a pure quaternion. The addition and multiplication of quaternions are similar to those of complex numbers, except that the multiplication of quaternions does not satisfy the commutative law, *i.e.*, in general $\dot{p}\dot{q} \neq \dot{q}\dot{p}$. The conjugate and the modulus of a quaternion \dot{q} are, respectively, defined as

$$\begin{aligned} \dot{q}^* &= q_0 - q_1i - q_2j - q_3k, \\ |\dot{q}| &= \sqrt{\dot{q}\dot{q}^*} = \sqrt{q_0^2 + q_1^2 + q_2^2 + q_3^2}. \end{aligned}$$

Analogously, a quaternion matrix $\dot{\mathbf{Q}} = (\dot{q}_{mn}) \in \mathbb{H}^{M \times N}$ is written as $\dot{\mathbf{Q}} = \mathbf{Q}_0 + \mathbf{Q}_1i + \mathbf{Q}_2j + \mathbf{Q}_3k$, where $\mathbf{Q}_l \in \mathbb{R}^{M \times N}$ ($l = 0, 1, 2, 3$), $\dot{\mathbf{Q}}$ is named a pure quaternion matrix when $\Re(\dot{\mathbf{Q}}) = \mathbf{Q}_0 = \mathbf{0}$. The quaternion matrix Frobenius norm and L_1 -norm are respectively defined as $\|\dot{\mathbf{Q}}\|_F = \sqrt{\sum_{m=1}^M \sum_{n=1}^N |\dot{q}_{mn}|^2}$ and $\|\dot{\mathbf{Q}}\|_{L_1} = \sum_{m=1}^M \sum_{n=1}^N |\dot{q}_{mn}|$. The quaternion singular value decomposition (QSVD) of $\dot{\mathbf{Q}}$ is defined by [32]: $\dot{\mathbf{Q}} = \dot{\mathbf{U}}\dot{\mathbf{\Sigma}}\dot{\mathbf{V}}^H$, where $\dot{\mathbf{U}} \in \mathbb{H}^{M \times M}$ and $\dot{\mathbf{V}} \in \mathbb{H}^{N \times N}$ are unitary quaternion matrices, $\dot{\mathbf{\Sigma}}$ contains all the singular values of $\dot{\mathbf{Q}}$.

Readers can find more details on quaternion algebra in [32], [44], [45].

ACKNOWLEDGMENT

This work was supported by The Science and Technology Development Fund, Macau SAR (File no. FDCT/085/2018/A2) and University of Macau (File no. MYRG2019-00039-FST).

REFERENCES

- [1] L. D. Lathauwer, B. D. Moor, and J. Vandewalle, "A multilinear singular value decomposition," *SIAM J. Matrix Anal. Appl.*, vol. 21, no. 4, pp. 1253–1278, 2000.
- [2] J. Liang, Y. He, D. Liu, and X. Zeng, "Image fusion using higher order singular value decomposition," *IEEE Trans. Image Process.*, vol. 21, no. 5, pp. 2898–2909, 2012.
- [3] K. S. Gurumoorthy, A. Rajwade, A. Banerjee, and A. Rangarajan, "A method for compact image representation using sparse matrix and tensor projections onto exemplar orthonormal bases," *IEEE Transactions on Image Processing*, vol. 19, no. 2, pp. 322–334, 2010.
- [4] R. Costantini, L. Sbaiz, and S. Susstrunk, "Higher order svd analysis for dynamic texture synthesis," *IEEE Transactions on Image Processing*, vol. 17, no. 1, pp. 42–52, 2008.
- [5] S. Gao, N. Guo, M. Zhang, J. Chi, and C. Zhang, "Image denoising based on HOSVD with iterative-based adaptive hard threshold coefficient shrinkage," *IEEE Access*, vol. 7, pp. 13 781–13 790, 2019.

- [6] B. Chen, Q. Liu, X. Sun, X. Li, and H. Shu, "Removing gaussian noise for colour images by quaternion representation and optimisation of weights in non-local means filter," *IET Image Processing*, vol. 8, no. 10, pp. 591–600, 2014.
- [7] X. Hu and K. I. Kou, "Phase-based edge detection algorithms," *Mathematical Methods in the Applied Sciences*, vol. 41, no. 11, 2018.
- [8] Y. Chen, X. Xiao, and Y. Zhou, "Low-rank quaternion approximation for color image processing," *IEEE Trans. Image Process.*, vol. 29, pp. 1426–1439, 2020.
- [9] Y. Yu, Y. Zhang, and S. Yuan, "Quaternion-based weighted nuclear norm minimization for color image denoising," *Neurocomputing*, vol. 332, pp. 283–297, 2019.
- [10] C. Zou, K. I. Kou, and Y. Wang, "Quaternion collaborative and sparse representation with application to color face recognition," *IEEE Trans. Image Processing*, vol. 25, no. 7, pp. 3287–3302, 2016.
- [11] C. Zou, K. I. Kou, L. Dong, X. Zheng, and Y. Y. Tang, "From grayscale to color: Quaternion linear regression for color face recognition," *IEEE Access*, vol. 7, pp. 154 131–154 140, 2019.
- [12] J. Miao and K. I. Kou, "Quaternion-based bilinear factor matrix norm minimization for color image inpainting," *IEEE Trans. Signal Process.*, vol. 68, pp. 5617–5631, 2020.
- [13] Z. Jia, M. K. Ng, and G. Song, "Robust quaternion matrix completion with applications to image inpainting," *Numer. Linear Algebra Appl.*, vol. 26, no. 4, 2019.
- [14] Y. Liu, L. Wang, J. Cheng, C. Li, and X. Chen, "Multi-focus image fusion: A survey of the state of the art," *Inf. Fusion*, vol. 64, pp. 71–91, 2020.
- [15] H. Li, B. S. Manjunath, and S. K. Mitra, "Multisensor image fusion using the wavelet transform," *CVGIP Graph. Model. Image Process.*, vol. 57, no. 3, pp. 235–245, 1995.
- [16] B. Yang, S. Li, and F. Sun, "Image fusion using nonsubsampling contourlet transform," in *International Conference on Image & Graphics*, 2007.
- [17] Z. Zhou, S. Li, and B. Wang, "Multi-scale weighted gradient-based fusion for multi-focus images," *Inf. Fusion*, vol. 20, pp. 60–72, 2014.
- [18] S. Li, X. Kang, and J. Hu, "Image fusion with guided filtering," *IEEE Trans. Image Process.*, vol. 22, no. 7, pp. 2864–2875, 2013.
- [19] X. Bai, Y. Zhang, F. Zhou, and B. Xue, "Quadtree-based multi-focus image fusion using a weighted focus-measure," *Inf. Fusion*, vol. 22, pp. 105–118, 2015.
- [20] X. Qiu, M. Li, L. Zhang, and X. Yuan, "Guided filter-based multi-focus image fusion through focus region detection," *Signal Process. Image Commun.*, vol. 72, pp. 35–46, 2019.
- [21] K. Zhan, L. Kong, B. Liu, and Y. He, "Multimodal image seamless fusion," *J. Electronic Imaging*, vol. 28, no. 02, p. 023027, 2019.
- [22] Y. Liu, X. Chen, H. Peng, and Z. Wang, "Multi-focus image fusion with a deep convolutional neural network," *Inf. Fusion*, vol. 36, pp. 191–207, 2017.
- [23] R. Lai, Y. Li, J. Guan, and A. Xiong, "Multi-scale visual attention deep convolutional neural network for multi-focus image fusion," *IEEE Access*, vol. 7, pp. 114 385–114 399, 2019.
- [24] Y. Liu, J. Jin, Q. Wang, Y. Shen, and X. Dong, "Region level based multi-focus image fusion using quaternion wavelet and normalized cut," *Signal Process.*, vol. 97, pp. 9–30, 2014.
- [25] P. Chai, X. Luo, and Z. Zhang, "Image fusion using quaternion wavelet transform and multiple features," *IEEE Access*, vol. 5, pp. 6724–6734, 2017.
- [26] Y. Liu, J. Jin, Q. Wang, Y. Shen, and X. Dong, "Novel focus region detection method for multifocus image fusion using quaternion wavelet," *J. Electronic Imaging*, vol. 22, no. 2, p. 023017, 2013.
- [27] H. Pang, M. Zhu, and L. Guo, "Multifocus color image fusion using quaternion wavelet transform," in *International Congress on Image & Signal Processing*, 2013.
- [28] L. Guo, M. Dai, and M. Zhu, "Multifocus color image fusion based on quaternion curvelet transform," *Optics Express*, vol. 20, no. 17, pp. 18 846–60, 2012.
- [29] X. Luo, Z. Zhang, C. Zhang, and X. Wu, "Multi-focus image fusion using HOSVD and edge intensity," *J. Vis. Commun. Image Represent.*, vol. 45, pp. 46–61, 2017.
- [30] J. Miao, K. I. Kou, and W. Liu, "Low-rank quaternion tensor completion for recovering color videos and images," *Pattern Recognit.*, vol. 107, p. 107505, 2020.
- [31] W. Rowan Hamilton, "Ii. on quaternions; or on a new system of imaginaries in algebra," *Phil. Mag., 3rd Ser.*, vol. 25, 01 1844.
- [32] F. ZHANG, "Quaternions and matrices of quaternions," *Linear algebra and its applications*, vol. 251, pp. 21–57, 1997.
- [33] T. G. Kolda and B. W. Bader, "Tensor decompositions and applications," *SIAM Rev.*, vol. 51, no. 3, pp. 455–500, 2009.
- [34] D. I. M. Johnstone, "Ideal spatial adaptation by wavelet shrinkage," *Biometrika*, vol. 81, no. 3, pp. 425–455, 1994.
- [35] S. Gu, Q. Xie, D. Meng, W. Zuo, X. Feng, and L. Zhang, "Weighted nuclear norm minimization and its applications to low level vision," *Int. J. Comput. Vis.*, vol. 121, no. 2, pp. 183–208, 2017.
- [36] M. Nejati, S. Samavi, and S. Shirani, "Multi-focus image fusion using dictionary-based sparse representation," *Inf. Fusion*, vol. 25, pp. 72–84, 2015.
- [37] M. Hossny, S. Nahavandi, and D. Creighton, "Comments on 'information measure for performance of image fusion'," *Electronics Letters*, vol. 44, no. 18, pp. 1066–1067, 2008.
- [38] Q. Wang, Y. Shen, and J. Q. Zhang, "A nonlinear correlation measure for multivariable data set," *Physica D-nonlinear Phenomena*, vol. 200, no. 3–4, pp. 287–295, 2005.
- [39] C. Yang, J. Q. Zhang, X. R. Wang, and X. Liu, "A novel similarity based quality metric for image fusion," *Information Fusion*, vol. 9, no. 2, pp. 156–160, 2008.
- [40] Y. Chen and R. S. Blum, "A new automated quality assessment algorithm for image fusion," *Image Vis. Comput.*, vol. 27, no. 10, pp. 1421–1432, 2009.
- [41] H. Chen and P. K. Varshney, "A human perception inspired quality metric for image fusion based on regional information," *Inf. Fusion*, vol. 8, no. 2, pp. 193–207, 2007.
- [42] Z. Liu, E. Blasch, Z. Xue, J. Zhao, R. Laganière, and W. Wu, "Objective assessment of multiresolution image fusion algorithms for context enhancement in night vision: A comparative study," *IEEE Trans. Pattern Anal. Mach. Intell.*, vol. 34, no. 1, pp. 94–109, 2012.
- [43] Z. Wang, A. C. Bovik, H. R. Sheikh, and E. P. Simoncelli, "Image quality assessment: from error visibility to structural similarity," *IEEE Trans. Image Processing*, vol. 13, no. 4, pp. 600–612, 2004.
- [44] P. R. Girard, *Quaternions, Clifford Algebras and Relativistic Physics*, 2007.
- [45] S. L. Altmann, "Rotations, quaternions, and double groups," *Acta Crystallographica*, vol. 44, no. 4, 1986.